J. Fluid Mech. (2000), *vol.* 412, *pp.* 259–277. Printed in the United Kingdom

Experimental study of secondary instability in a hypersonic shock layer on a flat plate

By S. G. MIRONOV AND A. A. MASLOV

Institute of Theoretical and Applied Mechanics SB RAS, 630090, Novosibirsk, Russia

(Received 7 July 1999 and in revised form 26 January 2000)

The development of secondary instability on streamwise vortex structures generated in a hypersonic shock layer on a flat plate is experimentally studied for the flow with Mach number $M_\infty = 21$ and unit Reynolds number $Re_1 = 6 \times 10^5\,\mathrm{m}^{-1}$. The study is performed using the electron-beam method. The generation of weak unsteady vortices and steady streamwise vortex structures with finite-amplitude perturbations imposed onto them is studied in detail. Complex data on the characteristics of density fluctuations developed on quasi-steady and unsteady streamwise vortex structures are obtained. It is shown that the characteristics of the natural fluctuations of density developing in the shock layer on a flat plate are qualitatively similar to density fluctuations induced by weak unsteady vortex perturbations introduced into the shock layer. The possibility of existence of parametric resonance between the fundamental frequency and its harmonic and between harmonics for steady streamwise vortex structure is shown.

1. General objectives and survey analysis

Experimental investigation of secondary instability is very important for the problem of the laminar–turbulent transition in the boundary layer. In particular, secondary instability has a significant effect on the process of breakdown of vortices that arise in the flow around swept wings and concave surfaces and on the transition to turbulence in the boundary layer. The basic studies in this direction were conducted for subsonic flows; a review of these studies can be found in Saric (1994) and Boiko *et al.* (1999). For hypersonic flows, there are only two theoretical papers, Fu & Hall (1992, 1993), devoted to the development of secondary instability in large-amplitude Görtler vortices. As has been shown by Fu & Hall (1993) the influence of Görtler vortices is not as pronounced as that of wall cooling or gas dissociation. The main effect of Görtler vortices is to increase the unstable band of Rayleigh waves, and thus the presence of large-amplitude vortices is likely to cause the boundary layer to become more receptive to transition induced by Rayleigh modes. The literature does not offer any data from experimental investigation of the characteristics of secondary instability for high Mach numbers, in particular for a hypersonic shock layer. However, the observation and investigation of secondary instability in a hypersonic shock layer seem particularly important, since the primary mechanisms of the loss of stability known for subsonic and supersonic flows are not manifested in the shock layer because of the large thickness of the layer and small velocity gradients. Therefore, secondary instability can be a dominating factor in inducing turbulence in a hypersonic boundary layer if there are considerable crossflow and transverse

gradients of the mean velocity, which are caused, in particular, by induced vortex structures.

The results of an experimental study of the characteristics of density fluctuations in a hypersonic shock layer on a flat plate in the presence of unsteady and quasi-steady vortex perturbations of the mean finite-amplitude flow field are presented in the paper.

2. Experimental equipment and measurement techniques

2.1. *Wind tunnel and flat-plate model*

The experiments were conducted in the hypersonic nitrogen wind tunnel T-327 of ITAM SB RAS. This facility is a continuous-operation open-type free-jet wind tunnel with gas efflux into a vacuum cavity with a volume of $100\,\mathrm{m}^3$, which is evacuated by mechanical pumps with a productivity of $6\,\mathrm{m}^3\,\mathrm{s}^{-1}$. The running time of the wind tunnel is 30 s. It is equipped with an electric gas heater and a system for shock starting. The diameter of the exit cross-section of a conical water-cooled nozzle is 0.22 m, the nozzle cone angle is 8°, and the diameter of the uniform-flow core is 0.1 m. The Mach number at the nozzle exit is equal to 20. The longitudinal gradient of the Mach number due to flow expansion in the test section is $\approx 3\,\mathrm{m}^{-1}$. The non-uniformity of the Mach number distribution over the flow core cross-section is less than 5% at the edge of the core. The measurements were performed in the test section of the wind tunnel, where the flow Mach number is $M_\infty \approx 21$, for the unit Reynolds number $Re_1 = 6 \times 10^5\,\mathrm{m}^{-1}$ and temperature factor $T_w/T_0 = 0.26$–0.29. The stagnation temperature was kept at 1100 K. For these conditions, the flow velocity was $U_\infty = 1480\,\mathrm{m\,s}^{-1}$ and the density (concentration) of nitrogen molecules was $n_\infty = 6.8 \times 10^{21}\,\mathrm{m}^{-3}$. The gas density decreases by more than an order of magnitude outside the flow core, at a distance of 0.02 m. From the data of electron-beam measurements and acoustic probing, the total intensity of density fluctuations in the flow core does not exceed 0.5%. Nevertheless, such a level of noise means that the installation cannot be classified as a 'quiet' wind tunnel.

The characteristics of density fluctuations were measured in the shock layer on a flat-plate model, which was a trapezium made of blackened aluminium with the following dimensions: the leading-edge width was 0.1 m, the trailing-edge width was 0.08 m, the length was 0.35 m, and the thickness was 0.008 m; the wedge angle at the leading edge was 7° and the radius of the edge bluntness was about 0.05 mm. The side edges of the plate were made as wedges with an angle of 20°.

2.2. *Principle of introduction of perturbations and construction of the source of perturbations*

The perturbations were introduced into the shock layer by the interaction of the leading edge of the flat plate with an oscillating shock layer generated by an oblique aerodynamic whistle (see figure 1, right-hand side). A photograph of the electron-beam visualization of the hypersonic flow around the flat-plate model with a whistle is shown in figure 2. As is shown by Maslov & Mironov (1996), the flow around the whistle is accompanied by periodic radial oscillations of the shock layer, which can be used to generate perturbations. In the region where the leading edge of the flat plate and the shock layer generated by the whistle cross, surface streamlines pass through two shock waves: the oblique shock wave of the whistle and the bow shock of the leading edge of the plate. In the region away from this crossing point, surface streamlines pass through only the bow shock. Because of that, a zone with a lower

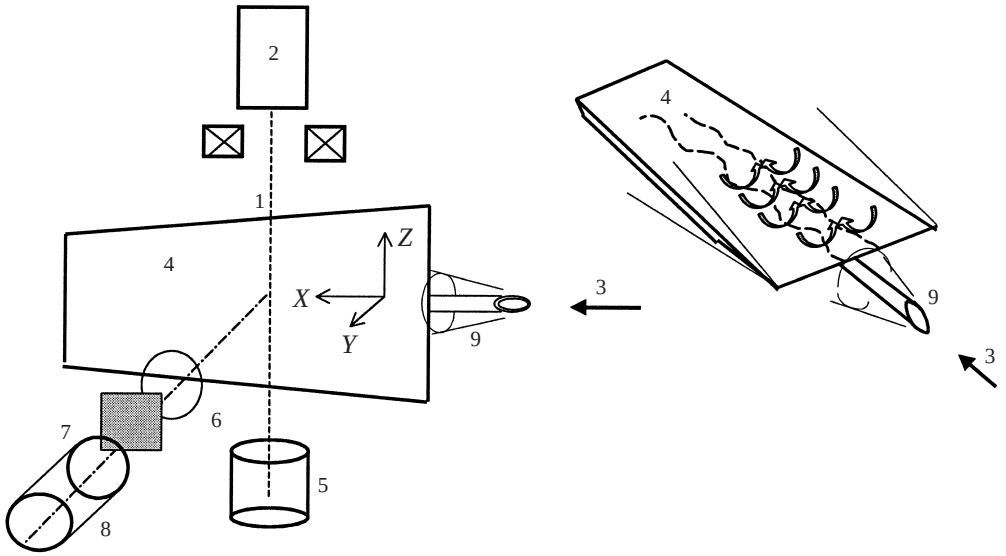

FIGURE 1. A schematic of electron-beam measurements and the introduction of perturbations into a hypersonic shock layer. 1 – electron beam; 2 – electron gun; 3 – hypersonic flow; 4 – flat-plate model; 5 – collector of electrons; 6 – lens; 7 – light filter; 8 – photomultiplier, 9 – oblique-cut whistle.

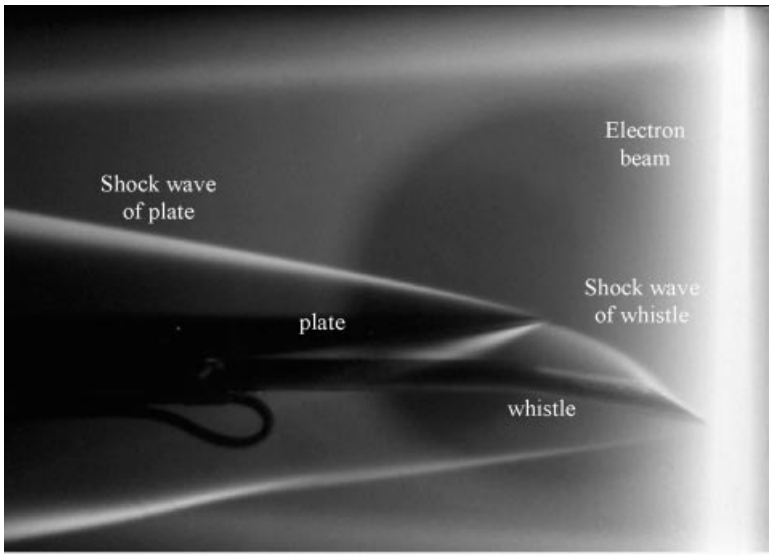

FIGURE 2. Electron-beam visualization of the flow field around the flat-plate model with a whistle.

static pressure is formed on the plate past the interaction region. Wavy dashed lines in figure 1 (right-hand side) show the boundaries of the low-pressure zone for an oscillating shock wave generated by the whistle.

Two-dimensional calculations within the framework of the full viscous shock layer model (Vetlutsky, Mironov & Poplavskaya 1996; Maslov *et al.* 1999) showed that the static pressure in the interaction region is three times lower than the pressure in the undisturbed region. This should lead to the motion of gas from the periphery to the plate centreline, the formation of a gas flow moving upward from the plate, and

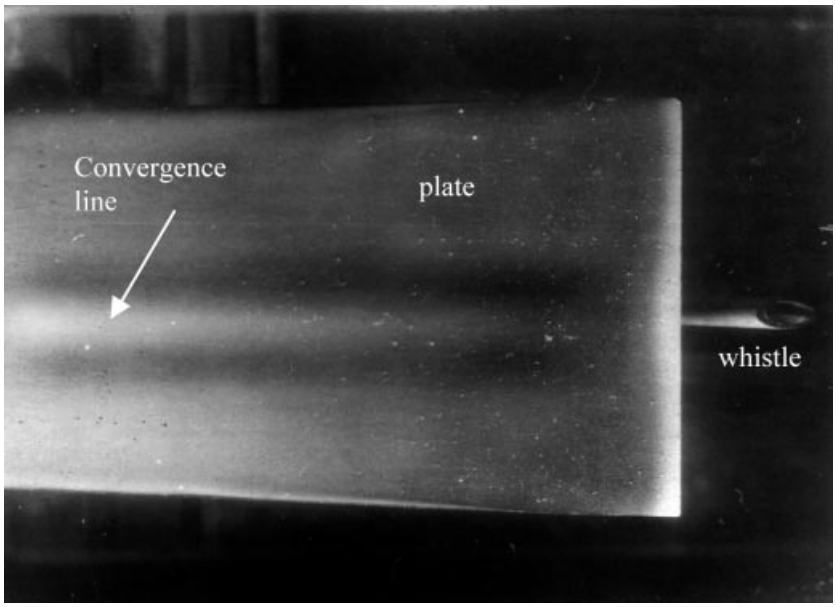

FIGURE 3. Visualization of the flow field on the plate surface using a film of oil and chalk powder.

the generation of a pair of counter-rotating vortices extended along the flow (arrows, figure 1, right-hand side). Depending on the depth of penetration of the flat-plate leading edge into the shock layer on the whistle and the amplitude of oscillations of the shock layer, it is possible to obtain both purely unsteady vortices and also quasi-steady vortex structures with oscillations imposed onto them. The formation of a pair of counter-rotating vortices can be illustrated by a photograph of flow visualization on the plate surface (figure 3), which was performed using the oil-film technique with chalk powder. The light stripe on the plate centreline corresponds to the convergence line, the two neighbouring dark stripes show the position of the maximum velocity of the transverse motion of the gas. The flow pattern in this picture corresponds to a quasi-steady interaction.

The construction of the whistle is described in Maslov & Mironov (1996). In the present work, the whistle was a copper tube 0.15 m long with external diameter 0.008 m and internal diameter 0.006 m and with an obliquely cut frontal face at an angle of 20° to the tube axis. A movable, tightly positioned piston with a probe for pressure fluctuations was located inside the tube. The tube was cooled by running water to maintain a constant temperature of the resonator walls. The perturbation frequency could be controlled by moving the piston along the tube. The distance between the tip of the whistle and the edge of the plate was 40 mm in the streamwise direction. The tube was located under the plate, pitched down at an angle of 8.5° to the free-stream direction. This angle ensured the maximum intensity of pressure fluctuations in the cavity of the whistle, equal to 140 dB at frequency 5–10 kHz. Preliminary distributions of the constant and variable components of the signal of the optical system were obtained during transverse scanning of the shock layer on the whistle by an electron beam in the cross-section corresponding to the position of the flat-plate leading edge. Based on these data and the technique described by Maslov & Mironov (1996), we estimated the amplitude of the shock-wave oscillations to be 0.2 mm. The character

of interaction could be controlled by varying the distance between the leading edge of the plate and the tube surface.

2.3. *Equipment and measurement technique*

The measurements were performed using the method of electron-beam fluorescence described by Maslov, Mironov & Shiplyuk (1996*a*). The measurement scheme is shown in figure 1. The probing electron beam (1) was generated by an electron gun (2), which had a magnetic system for controlling the beam position. The electron beam propagated across a hypersonic flow (3) parallel to the flat-plate surface (4). The current in the beam was controlled by the current to an electron collector (5) located outside the flow. The optical system of nitrogen fluorescence registration consisted of a fast lens (6), light filter (7), and photomultiplier (8). The coordinate system is shown in the figure. The X-scanning of the measurement point was performed by moving the plate along the flow centreline within the range of $-5\ldots+210$ mm relative to the electron beam position. The scanning of the measurement point along the Y-coordinate, which passes across the shock layer, was performed by moving the plate across the flow within the range of $-15\ldots+15$ mm from the flow centreline. The scanning along the transverse coordinate Z was performed by moving the optical system for fluorescence registration (the point of observation) along the axis of the electron beam within the range of $-20\ldots+50$ mm from the axis of symmetry of the plate. Control measurements on a motionless model, which were performed by scanning the flow field with a moving electron beam, showed that those results coincided with the data obtained by moving the flat plate. The spatial resolution of the optical system was 2 mm in the X- and Z-directions, and along the Y-coordinate it was determined by the width of fluorescence and was ≈ 3 mm.

The mean density was recovered from the values of the mean component of the photomultiplier signal by means of the calibration characteristic of the optical system, which relates the fluorescence intensity to the density at the measurement point (Maslov & Mironov 1998). The accuracy of mean density measurements was better than 5%.

All measurements were made at the position of the maximum of density fluctuations in the shock layer. The measurements showed that the positions of the maximum fluctuations coincide with the line $Y = 0.75\Delta$ (Δ is the shock-wave position relative to the surface, which was obtained from flow visualization on the plate using an electron beam). The positions of the maximum fluctuations corresponded within 10% to the equal mean-density line in the shock layer on the flat plate. As has been shown by Maslov & Mironov (1998), this allows the characteristics of density waves to be received directly from the fluctuating component of the photomultiplier signal.

2.4. *Processing technique*

All measurements were performed for the fixed fundamental frequency of pressure pulsations in the cavity of the whistle $f = 8.5$ kHz, and two first harmonics and the subharmonic of this pulsation. For the test conditions, the frequency f corresponds to the frequency parameter $F = 0.6 \times 10^{-4}$ ($F = 2\pi f / Re_{1e} U_e$, where Re_{1e}, U_e are the unit Reynolds number and the gas velocity calculated from the parameters behind the shock wave on the plate).

At the first stage of processing the fluctuating component of the photomultiplier signal, the fast Fourier transform of temporal data arrays was used to calculate the cross-spectra (amplitude and phase spectra) between the fluctuations of fluorescence intensity and the reference signal. The pressure fluctuations in the whistle (signal

of the pressure probe) served as a reference signal. This allowed one to eliminate the effect of the stochastic noise of the low-intensity photocurrent and wide-band natural density fluctuations in the shock layer on the flat plate. The cross-spectra were averaged on 64 transforms of independent temporal data samples. In addition, the coherence spectra (normalized cross-spectra) were calculated. These spectra were used to estimate statistical errors of definition of the amplitude and phase (Bendat & Piersol 1980). Under the present test conditions, statistical fluctuations are the main source of measurement data errors.

Normalization of the amplitude cross-spectra by the square root of the electron-beam current and the reference signal intensity helped to minimize the effect of variation of these parameters on the measurement results. The amplitude measurements in the transverse direction Z were corrected to account for the attenuation of the signal of the optical system, which is related to scattering of electrons in the gas. The signal attenuation characteristics were determined by measurements on the flat-plate model without the whistle, as described by Vetlutsky *et al.* (1995).

Since there was no subharmonic in the pressure fluctuation spectrum in the whistle, the cross-spectra for the subharmonic frequency were calculated using the reference signal obtained by halving the fundamental frequency of pressure fluctuations in the whistle. This allows one to identify slow variations of the fundamental frequency, which is important for determining the phase of fluctuations.

After that, the amplitude and phase spectra versus the transversal wavenumbers β ($\beta = 2\pi/\lambda_Z$, where λ_Z is the wavelength in the transverse direction Z) were calculated at several X-stations using Hamming's spectral window. Previously, measurements had been symmetrized relative to the centreline of the plate ($Z = 0$). β-spectra were calculated from the relation

$$A(\beta)\exp[\mathrm{i}\phi(\beta)] = \int_{-Z_0}^{Z_0} A(z)\exp[\mathrm{i}\phi(z)]\exp[-\mathrm{i}\beta z]\partial z. \tag{1}$$

Here A, ϕ are the amplitude and phase of density fluctuations; $-Z_0, Z_0$ are the coordinates of the side edges of the plate. The method of expansion on transversal wavenumbers reveals the existence of inclined waves of density, to determine the phase velocity and increment from the inclination angle.

Based on the resultant spectra, the longitudinal phase velocities of propagation of the density waves C_X and the growth rates $-\alpha_i$ for the fundamental frequency and harmonics were determined using the least-squares technique. The angles of inclination of the wave vector to the stream direction χ were calculated from the values of the transverse β and longitudinal α wavenumbers. The angle χ was calculated from the relation

$$\chi = a\tan\left(\frac{\beta}{\alpha}\right); \quad \alpha = \frac{2\pi f}{C_X U_e}.$$

Application of the β-spectra reduces a statistical error in the definition of the spectral amplitude and phase (consequently, phase velocity and increment), as when evaluating spectra, values containing an accidental error are summed (see relation (1)). Also, random fluctuations in the amplitude of spectra are shifted in regions of large wavenumbers (large angles of inclination of waves).

In the present paper the error in the definition of amplitude and phase of β-spectra was calculated by the method of direct numerical simulation. Thus for each β-spectrum ten new β-spectra were calculated. These spectra were calculated for values of amplitude $\bar{A}(z)$ and phase $\bar{\phi}(z)$ randomly differing from the measured values of

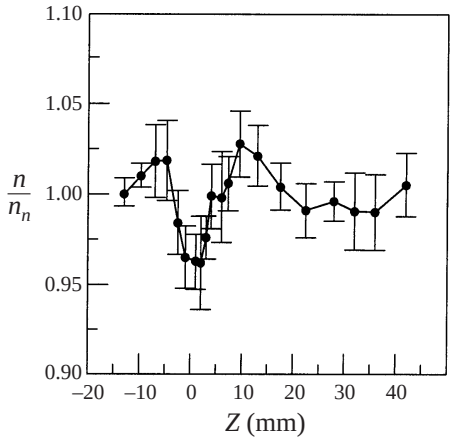

FIGURE 4. Deformation of the mean-density field. The results are averaged along the plate.

$A(z)$ and $\phi(z)$ from density fluctuations by a statistical error defined earlier using the coherence spectra. Then, to each value of amplitude and phase of the initial β-spectrum an error, corresponding to the maximum deviation of these values in the ensemble of the ten additional spectra at the same wavenumber, was added.

The calculations have shown that the error in the amplitude and phase of the β-spectrum (in the range $-1 \leqslant \beta \leqslant 1$ rad mm^{-1}) decreases approximately proportionally to $(N/2)^{1/2}$. Here N is the number of measurements along the Z-axis. The values of these errors were used to estimate the error of definition of the phase velocity and increment.

3. Measurement results

Two regimes of interaction between the flat-plate leading edge and the shock layer on the whistle were studied in detail in these experiments: (i) the generation of unsteady vortices; and (ii) the formation of a steady pair of vortices with fluctuations imposed onto them.

(i) *Unsteady vortices*

When the plate leading edge is placed at the depth of only 0.1 mm into the shock layer of the whistle, the amplitude of the shock-wave fluctuations exceeds this depth so that a vortex is formed only in part of the fluctuation period. This depth is the maximum distance between the line of the plate leading edge and the outer surface of the conical shock wave from the whistle in the region where they cross. The vortex motion of the gas leads to a weak deformation of the mean-density field. Figure 4 shows the transverse distribution of density n/n_n averaged over all X cross-sections. The density of molecules n is normalized by the density in the undisturbed shock layer n_n at the measurement point, and the error bars in the graph show the root-mean-square scatter of the measurement data over the cross-sections. It is seen that the distortion of the mean-density field does not exceed 5%. The character of this distortion corresponds to a pair of counter-rotating vortices, since the region of lower density on the plate centreline is correlated with two regions of higher density located outside the centreline, which confirms the assumption about the mechanism of the generation of perturbations. An oscillogram of perturbations at the fundamental

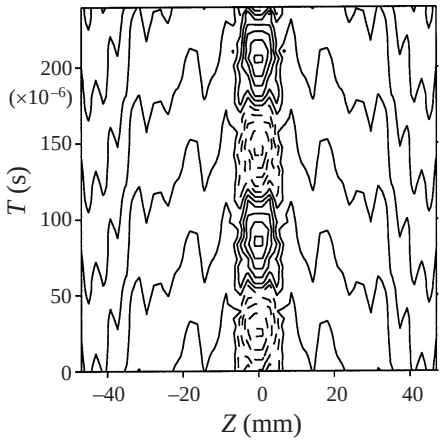

FIGURE 5. Oscillogram of the field of density fluctuations in the cross-section $X = 60$ mm at the fundamental frequency. The solid curves correspond to positive values of the deviation from mean density, the dashed curves refer to negative values.

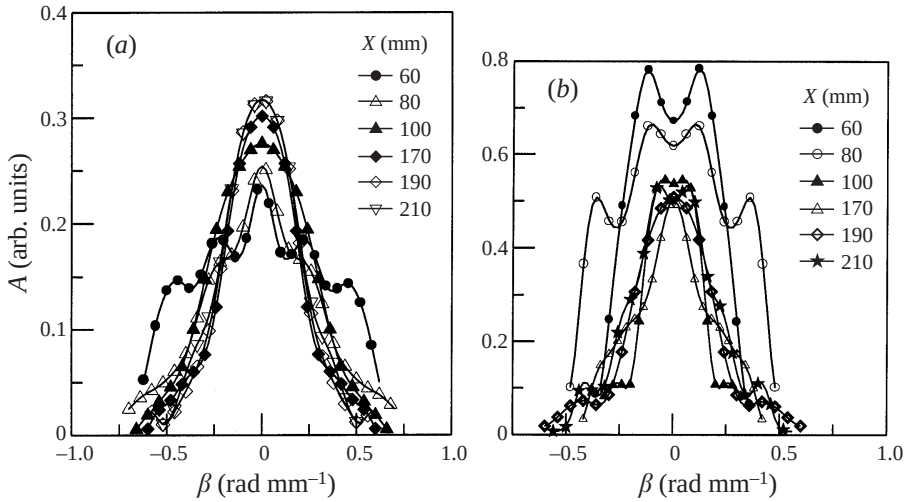

FIGURE 6. Amplitude β-spectra of density fluctuations at several X cross-sections: (*a*) fundamental frequency; (*b*) first harmonic.

frequency at a cross-section 60 mm from the plate leading edge is shown in figure 5. The solid isolines refer to positive values of density fluctuations, and the dashed curves show negative values. A comparison of the plots in figures 4 and 5 shows that the region of fluctuations corresponds to the region of deformation of the mean-density field.

The amplitude of fluctuations normalized by the free-stream density n'/n_∞ varied from 0.1% to 0.2% along the plate. It is seen from the amplitude (figure 6*a*, *b*) and phase (figure 7*a*, *b*) β-spectra obtained at several cross-sections that quasi-two-dimensional perturbations with the base width of $\approx \pm 0.5\,\mathrm{rad\,mm^{-1}}$ for the fundamental frequency and the first harmonic with a maximum at $\beta = 0$ are observed in the flat-plate shock layer. Based on the phase β-spectra calculated in the range $X = 60$ to 210 mm, we obtained the longitudinal phase velocities of the perturbations

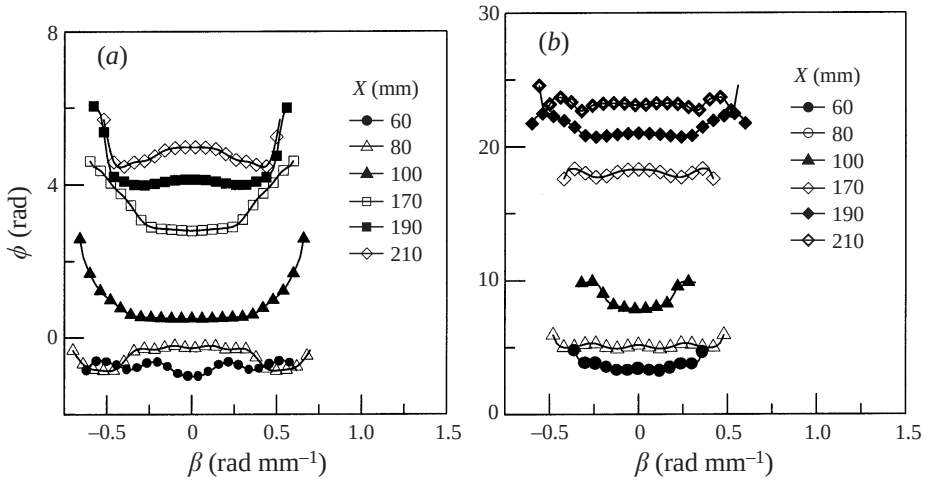

FIGURE 7. Phase β-spectra of density fluctuations at several X-stations: (*a*) fundamental frequency; (*b*) first harmonic.

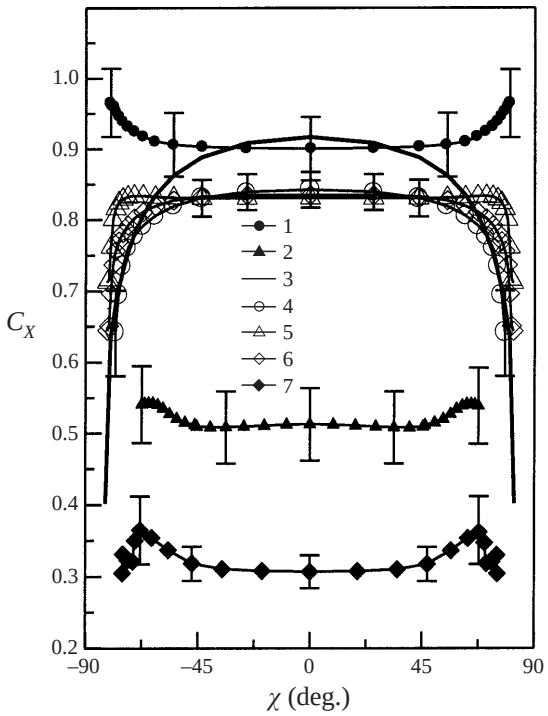

FIGURE 8. Spectra of the longitudinal phase velocity C_X of the density waves versus the angle of inclination of the wave vector to the stream direction χ. Case (i): 1 – fundamental frequency; 2 – first harmonic; 3 – function $1 - 1/(M_e \cos \chi)$. Case (ii): 4 – fundamental frequency; 5 – first harmonic; 6 – second harmonic; 7 – subharmonic.

C_X. It was found that the longitudinal phase velocity is constant along the plate and depends only on the wavenumber β. In a narrow region near the plate edge ($X < 30$ mm), the phase velocity decreases to a value close to 0.3, which agrees with the data of Maslov, Mironov & Shiplyuk (1996*b*), in which the region near the plate

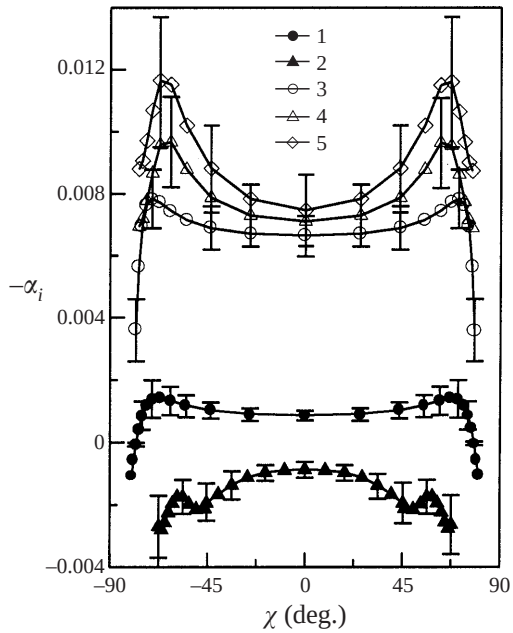

FIGURE 9. Spectra of the growth rate of the density waves $-\alpha_i$ versus the angle of inclination of the wave vector to the stream direction χ. Case (i): 1 – fundamental frequency; 2 – first harmonic. Case (ii): 3 – fundamental frequency; 4 – first harmonic; 5 – second harmonic.

edge where the formation of vortices occurs was studied. Curves 1 and 2 in figure 8 show the longitudinal phase velocity as a function of the angle of inclination of the wave vector to the stream direction $C_X(\chi)$ for the fundamental frequency and the first harmonic, respectively. (The parameters of the second harmonic and subharmonic in case (i) were not measured, since their amplitude was lower than the threshold value of the measurement system.) The velocity is normalized by the gas velocity behind the shock wave U_e. For comparison, curve 3 shows $1 - 1/(M_e \cos \chi)$. Here M_e is the Mach number behind the shock wave. According to the linear theory of stability of compressible flows (Mack 1969), perturbations with phase velocity lower than this curve belong to the acoustic mode, and those with phase velocity higher than this curve belong to the vortex mode. It is seen from figure 8 that, within the angle of $\pm 20^\circ$, the perturbations at the fundamental frequency propagate as acoustic vibrations. For higher angles, most probably, vortex perturbations are observed. The longitudinal phase velocity at the harmonic frequency was significantly lower and corresponded to the acoustic mode for all angles.

Based on the amplitude of the β-spectra, the standard procedure was applied to calculate the growth rates $-\alpha_i$. Curves 1 and 2 in figure 9 show the growth rate versus the angle of wave propagation $-\alpha_i(\chi)$ for the fundamental frequency and first harmonic, respectively. It is seen that the perturbations at the fundamental frequency increase and those at the first harmonic frequency decay.

(ii) *Quasi-steady vortices*

When the plate edge is placed at the depth of 1.2 mm into the shock layer of the whistle, a quasi-steady regime of interaction is observed. It is accompanied by the formation of a region of significant deformation of the mean flow field along the plate, seen in the visualization of figure 3. Figure 10(*b*) shows the mean-density distribution

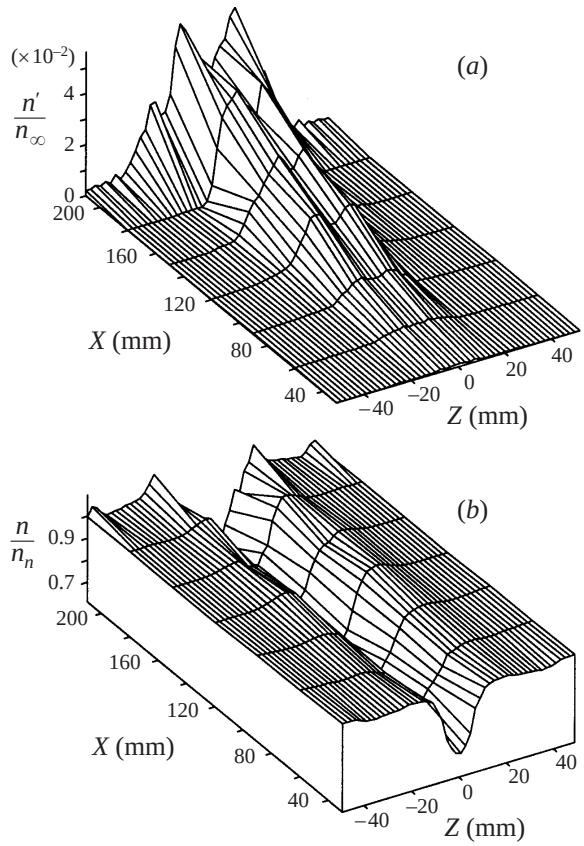

FIGURE 10. (*a*) Distribution of the amplitude of density fluctuations; (*b*) distribution of the deformation of the mean-density field in the maximum of fluctuations in the Y-direction in the flat-plate plane.

n/n_n on the plate. It is seen that the deformation of the mean flow field increases slightly downstream and reaches 40%. The character of the density deformation also corresponds to the propagation of a pair of vortices, since the region of lower density is correlated with the regions of higher density.

The asymmetry of the density field deformation along the normal coordinate relative to the density in the undisturbed shock layer in figure 10(*b*) is related to the nonlinear character of the mean-density distribution on the plate along the Y-axis at $Y \approx 0.75\Delta$. The measured mean-density distributions on the plate in the absence of vortex disturbances are shown in figure 11. The calculated mean characteristics of the flow field in the undisturbed shock layer (velocity, temperature, pressure) are presented by Vetlutsky *et al.* (1995, 1996). The maximum deviations of density from the undisturbed value correspond to a shift of the shock layer by $\approx$ 3%–5% of its thickness Δ away from the plate (the region of lower density) and by the same value toward the plate (the region of higher density). Estimates of the deformation of the mean-velocity field in the shock layer yield $\approx$ 5% of the undisturbed value. It should be noted that in case (i) the distortions of the mean-density field are rather small and, therefore, symmetric (the deformation of the mean-velocity field does not exceed $\approx$ 0.6%).

The amplitude of disturbances n'/n_∞ rapidly increases along the plate from 0.6% to

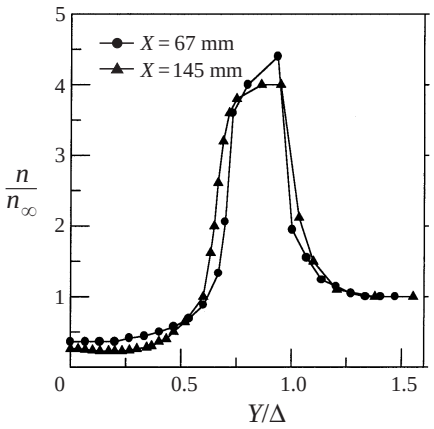

FIGURE 11. Mean-density distributions in the shock layer at $X = 67$ and 145 mm.

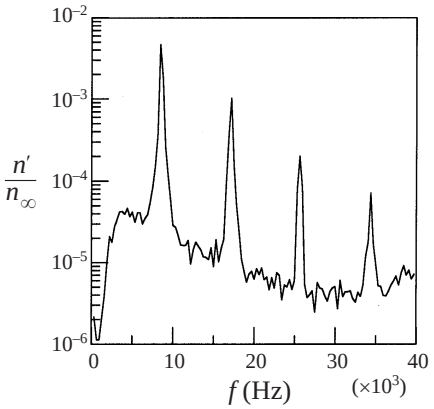

FIGURE 12. Frequency spectrum in the region of the maximum density fluctuations at the cross-section $X = 210$ mm.

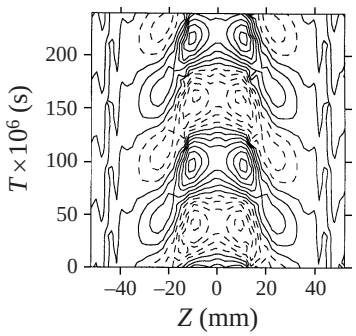

FIGURE 13. Oscillogram of the field of density fluctuations in the cross-section $X = 210$ mm at the fundamental frequency. The solid curves correspond to positive values of the deviation from mean density, the dashed curves refer to negative values.

6% in the range $X = 30$ to 210 mm (see figure 10*a*). A typical frequency spectrum and oscillogram of the transverse distribution of density fluctuations is shown in figures 12 and 13 for the cross-section $X = 210$ mm. A comparison of data in figures 10(*a*, *b*) and 13 shows that there are two maxima of fluctuations corresponding to the slopes

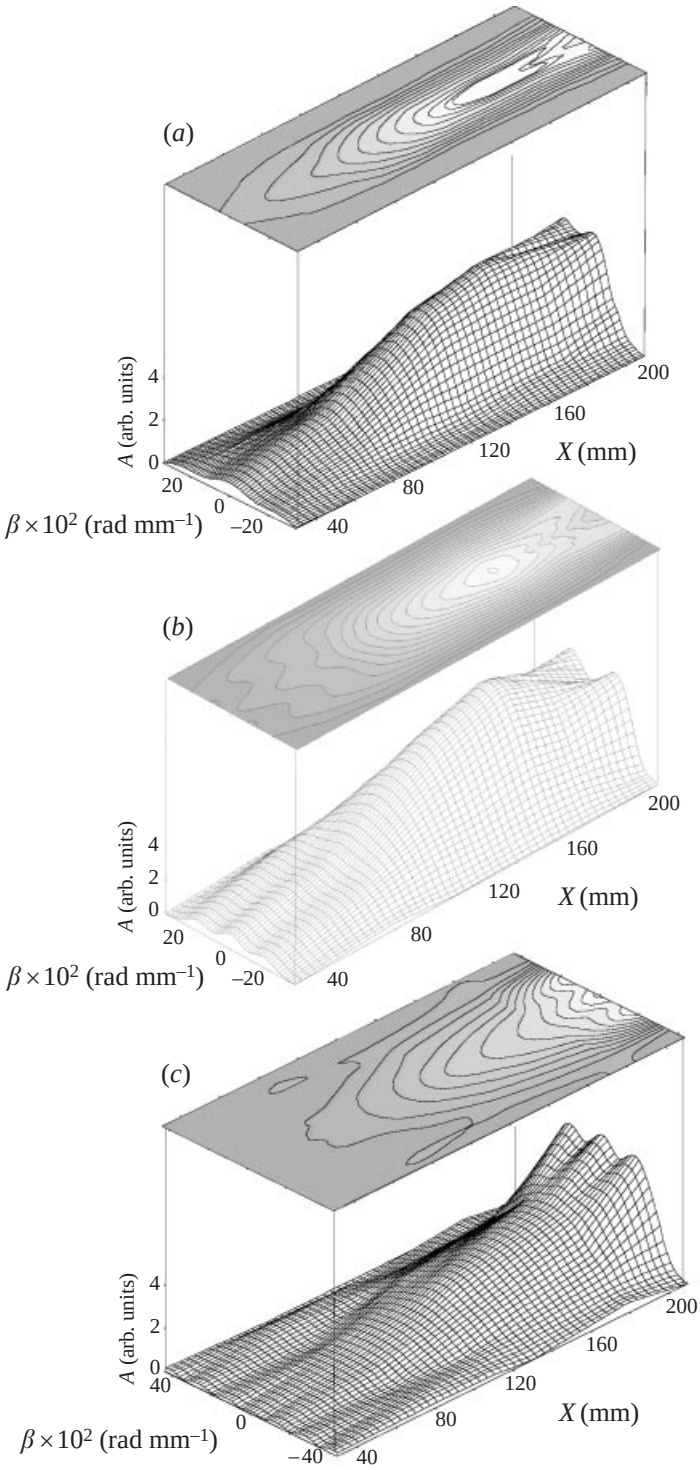

FIGURE 14. Amplitude β-spectra of density fluctuations: (*a*) fundamental frequency; (*b*) first harmonic; (*c*) second harmonic.

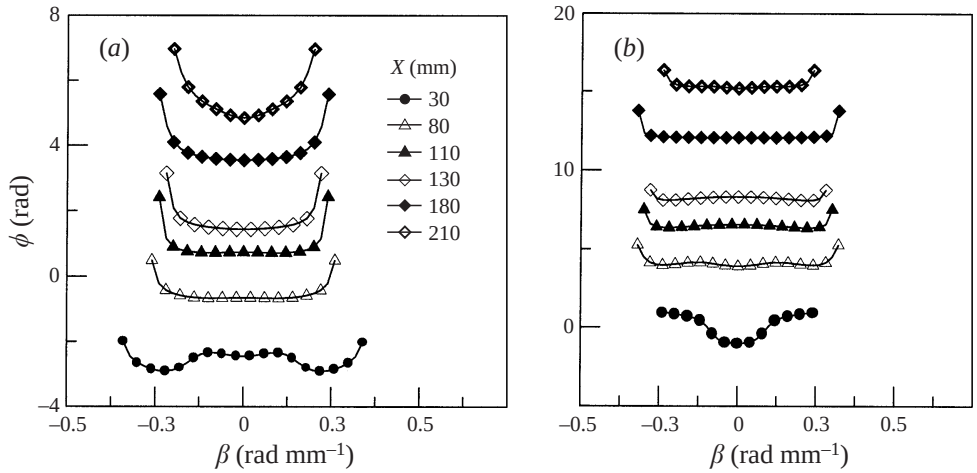

FIGURE 15. Phase β-spectra of density fluctuations at several X cross-sections: (a) fundamental frequency; (b) first harmonic.

of the low-density region, and the phase of fluctuations jumps by 180° on passing from the region of decreasing mean density to the region of increasing mean density. The intensity of fluctuations in high-density regions turned out to be significantly lower.

The amplitude and phase β-spectra in figures 14(a, b, c) and 15(a, b) show that quasi-two-dimensional perturbations with base width of $\approx \pm 0.25\,\mathrm{rad\,mm^{-1}}$ at the fundamental frequency and at the harmonic frequencies, with a maximum at a wavenumber equal to zero, are also observed in this case. For the X-coordinate in the range from 30 to 210 mm, the longitudinal phase velocities depend only on the transverse wavenumber. For distances smaller than 30 mm from the leading edge, the phase velocity, as in the previous case, decreases to a value close to 0.3, which is most probably connected with the existence of a transitional flow region at the edge (Maslov *et al.* 1996*b*). Figure 8 shows the longitudinal phase velocity C_X as a function of the angle of inclination of the wave vector to the stream direction χ for the fundamental frequency (curve 4) and the first and second harmonics (curves 5 and 6). In this case, the phase velocities are close to each other and correspond to the acoustic mode of disturbances.

In contrast to case (i), the dependence of the amplitude β-spectra on the longitudinal coordinate, for distances of more than $\approx$ 130 mm from the edge, cannot be described by a simple exponential curve because of the decrease in the growth rate of disturbances, which indicates a possible nonlinear stage of evolution of disturbances. In this connection, the growth rates for case (ii) were calculated only in the interval $X = 30$–130 mm. Curves 3, 4, and 5 in figure 9 show the growth rates at the fundamental frequency and harmonics versus the angle χ. The growth rates at three frequencies turned out to be close to each other and significantly greater than in case (i). A certain increase in the growth rate in passing from the fundamental frequency to a higher harmonic should be noted. At the end of a set of measurements, in the region of strong nonlinearity of amplitude growth (see figure 14) of the fundamental frequency and frequency of harmonics, it is possible to see the appearance of two symmetrical peaks.

To determine possible mechanisms for the appearance of nonlinearity in the de-

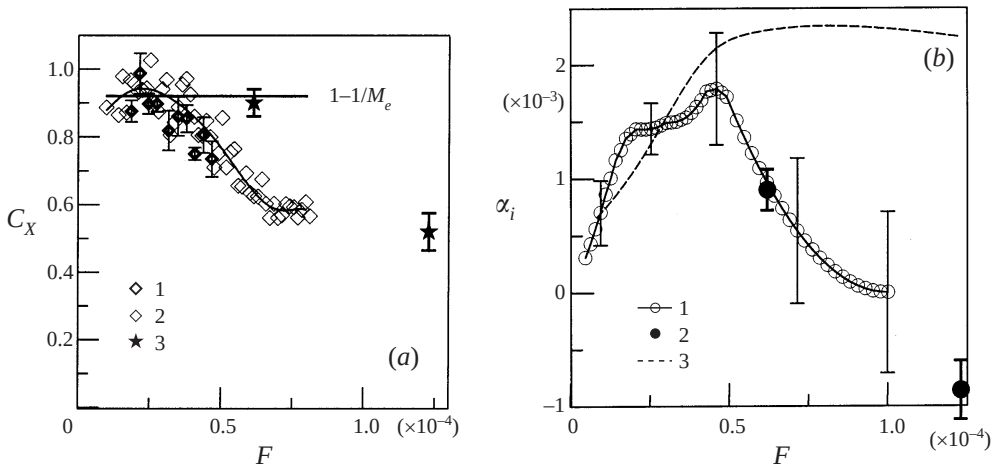

FIGURE 16. (*a*) Comparison of the longitudinal phase velocities. Natural disturbances: 1 – $X = 73$ mm; $Re_1 = 6\times10^5$ m^{-1}; 2 – $X = 300$ mm; $Re_1 = 9.5\times10^5$ m^{-1}. 3 – Secondary disturbances (case (i)), the longitudinal phase velocities (fundamental frequency and harmonic) determined in the range $X = 30$–210 mm. (*b*) Comparison of the growth rates of the density waves. 1 – Spectrum of increment of natural disturbances, determined in the range $X = 45$–100 mm at $Re_1 = 6\times10^5$ m^{-1}; 2 – increments of secondary disturbances (case (i)), determined in the range $X = 30$–210 mm; 3 – computational data.

velopment of secondary instability, the characteristics of the density waves at the subharmonic frequency were measured. Since the subharmonic was extracted from the integral signal for a constant level of the reference signal, which is not related in amplitude with the process under study, only the phase β-spectra are fully informative. The amplitude β-spectra allow only a qualitative estimate of the spectrum shape. It was found that they occupy a wide range of transverse wavenumbers with a weak maximum at $\beta = 0$, which corresponds to a narrow wave packet in the Z-direction. The longitudinal phase velocity C_X of fluctuations at the subharmonic frequency, which was calculated on the basis of phase spectra, is shown by curve 7 in figure 8.

4. Discussion of results

Since the results of the present study are novel for hypersonic viscous flows, it is of interest to compare them with the known experimental data on the secondary instability of streamwise vortex structures and the data on the evolution of natural disturbances in a hypersonic shock layer on a flat plate.

We should note the coincidence of the maximum disturbance intensities with the regions of the maximum mean-density gradient where the mean-velocity gradient is in the Z-direction. A similar phenomenon is mentioned in the review by Saric (1994) and experimentally confirmed for subsonic flows in Bakchinov *et al.* (1995), Boiko *et al.* (1995*a*, *b*, 1997), Levchenko & Shcherbakov (1997). The intensity of disturbances is higher in the upward flow from the plate, which is in agreement with the data of Levchenko & Shcherbakov (1997). The fact that the growth rates in case (ii) are greater than in case (i) by almost an order of magnitude is most probably related to the presence of a high mean-velocity gradient along the normal and transverse coordinates and, as a consequence, to the manifestation of viscous instability of the flow.

The characteristics of the waves of secondary instability (the longitudinal phase velocity and the growth rate) are compared in figure 16(a, b) for case (i) of the present study and the corresponding data for natural perturbations of density in a hypersonic shock layer on a flat plate. On figure 16(b) the result of the calculation of the fluctuations increment is shown (dashed line). It was derived according to the model proposed by Blackaby, Cowley & Hall (1993) for the same experimental conditions as the present paper. Fu & Hall (1993)'s results for Prandtl number $Pr = 0.72$ were used. The technique for obtaining the characteristics of natural perturbations and some results can be found in Maslov & Mironov (1998), and Maslov, Mironov & Shiplyuk (1998). It is quite possible that the difference between 1 and 3 in figure 16(b) is related to the influence of strong viscous–inviscid interaction in the shock layer.

For conditions (i), the mean-flow-field perturbations are rather small, as are the amplitudes of the moving perturbations of density, which allows a comparison with the results for natural perturbations. For the fundamental frequency and the first harmonic of vortex disturbances, the characteristics were compared within the range of angles $\chi = \pm 20°$, since the angle of propagation of natural perturbations does not exceed this value (Maslov *et al.* 1998). It is seen in figure 16(a) that the behaviour of the longitudinal phase velocity is qualitatively similar, its value for vortex disturbances decreases with increasing frequency, and its values correspond to the acoustic mode of disturbances. The coincidence is better for the growth rate, particularly for the fundamental frequency. It can be concluded that the introduction of vortex disturbances for the conditions of case (i) quite adequately simulates the process of penetration and development of natural external-flow perturbations in the shock layer.

It is worth mentioning that the position of the maxima of secondary fluctuations agrees with the position of the temperature adjustment layer (Blackaby *et al.* 1993; Fu & Hall 1993), where the temperature changes rapidly from its large value in the viscous layer to its free-stream value (quite the contrary occurs for density, see figure 11). This layer is the most dangerous site for Rayleigh instability.

The increase of the growth rates of density pulsations for a wide frequency band (at the fundamental frequency and harmonics), caused by a high-amplitude vortex, qualitatively agrees with the results of Fu & Hall (1993).

The nonlinearity in the development of secondary instability in case (ii) (figure 14) is not related to energy transfer from the fundamental frequency to the subharmonic. A comparison of the longitudinal wavenumbers α at the fundamental frequency ($\alpha_f = 0.042\,\mathrm{rad\,mm^{-1}}$) and subharmonic ($\alpha_s = 0.059\,\mathrm{rad\,mm^{-1}}$) shows that it is impossible to make a combination of them that would satisfy the parametric resonance condition. The process of the initial growth of harmonics and subsequent parametric resonance between the fundamental frequency and the first harmonic is possibly observed in case (ii), wherein the fundamental frequency acts as the subharmonic. Similar processes are also possible for harmonics whose frequency differs by a factor two. This four-wave mechanism was first proposed by Craik (1971) and developed by Nayfeh & Bozatli (1979). This mechanism was first experimentally shown and studied for subsonic boundary layers by Kachanov (1987, 1994). In this case, the β-spectra of the fundamental frequency and harmonics should have symmetric peaks about the zero wavenumber, which correspond to three-dimensional waves, which is observed in experiment (see the last cross-sections of β-spectra in figure 14). Based on the parametric resonance conditions and approximate equality of phase velocities of the perturbations, the positions of the maxima of these peaks on the β-axis should be close to the longitudinal wavenumbers α of those perturbations that act as the subharmonic in this process: $\beta \approx \pm 0.04$ for the fundamental frequency, $\beta \approx \pm 0.085$

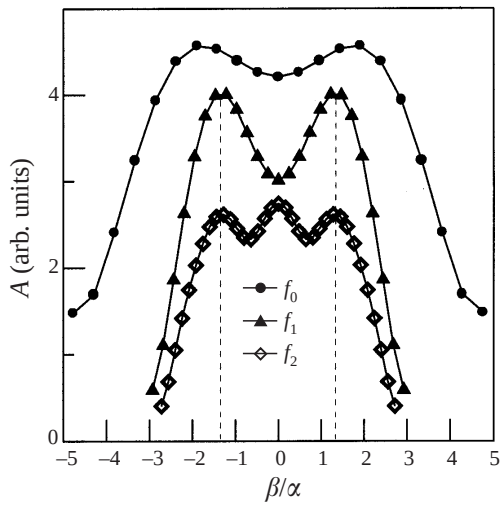

FIGURE 17. β-spectra obtained for the fundamental frequency (f_0), first harmonic (f_1) and second harmonic (f_2) versus the ratio of transverse β to longitudinal α wavenumbers. $X = 210$ mm (case (ii)).

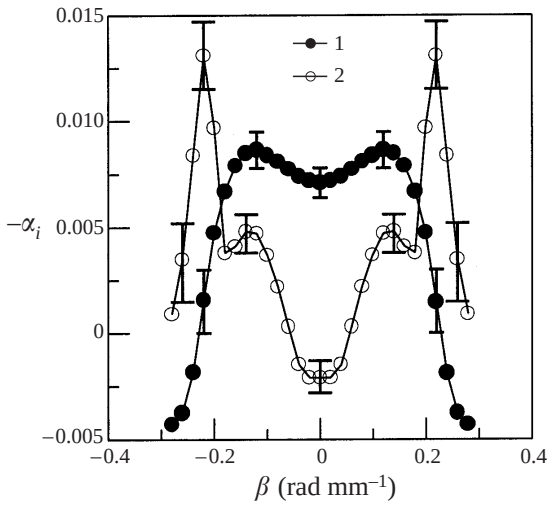

FIGURE 18. β-spectra of the increment of pulsations at the fundamental frequency calculated in the cross-sections $X = 30$ to 130 mm (1) and $X = 180$ to 210 mm (2) (case (ii)).

for the first harmonic, $\beta \approx \pm 0.125$ for the third harmonic, etc. and β/α is close to unity. The experimental positions of the maxima in the last cross-sections in figure 17 are quite close to these values. Apparently, the appearance of phase dependence for transversal wavenumber β in the last cross-section in figure 15(*a*) is connected to the formation of two inclined waves at the fundamental frequency.

The β-spectra of increment of pulsations at the fundamental frequency calculated in the ranges $X = 30$ to 130 mm and $X = 180$ to 210 mm are shown in figure 18. It is seen that growth of inclined waves takes place in the last cross-sections of the measurement section. The dependences in figures 17 and 18 are similar to the dependences obtained by Kachanov (1987, 1994) for K-regime transition of a

subsonic boundary layer, where the existence of the parametric resonance and the transformation of a two-dimensional wave into two oblique waves was shown.

The experimentally observed generation of harmonics and the similarity of the longitudinal phase velocity and the growth rates of the secondary instability frequency spectrum for the case of strong disturbances (ii) can be explained within the framework of the model proposed by Kimmel & Kendall (1991). According to this model, the harmonics are generated by transverse oscillations of a hypersonic boundary layer with a significantly non-monotonic normal distribution of the gas dynamic parameters, i.e. velocity or density (see figure 11). The harmonics arise in the regions of the maxima of the corresponding derivatives of the distributions with respect to the normal coordinate Y and transverse coordinate Z. This produces a natural relationship between the propagation velocity of the harmonics and their growth rates and the velocity and growth rate of disturbances at the fundamental frequency.

5. Conclusion

Experiments on unsteady and quasi-steady interaction of the shock layer from an oblique whistle and the flat-plate edge were conducted in a low-density hypersonic flow for Mach number 21 and unit Reynolds number $6 \times 10^5\,\mathrm{m}^{-1}$. A vortex motion of the gas in the flat-plate shock layer is demonstrated. The deformation of the mean-density field and the characteristics of moving disturbances at the fundamental frequency, two first harmonics and subharmonic are measured. The longitudinal phase velocities and the growth rates of disturbances versus the angle of wave propagation to the stream direction are obtained for two cases of interaction. A significant difference in these characteristics in these two cases of unsteady and quasi-steady interaction is shown. The measurement results are compared with some data obtained for subsonic flows, the results for natural perturbations in a hypersonic shock layer, some results of the linear theory of the stability of compressible flows, and models of the nonlinear stage of the evolution of perturbations in the boundary layer. It is shown that some characteristics of density fluctuations induced by weak unsteady vortex perturbations are qualitatively similar to the natural fluctuations of density developing in the shock layer on a flat plate. The possibility of the existence of four-wave parametric resonance between the fundamental frequency and the first harmonic and between the harmonics for steady streamwise vortex structure is shown.

The work was supported by the Russian Foundation for Basic Research (grant No. 98-01-00462).

REFERENCES

Bakchinov, A. A., Grek, G. R., Kligmann, B. G. B. & Kozlov, V. V. 1995 Transition experiments in a boundary layer with embedded streamwise vortices. *Phys. Fluids* **7**, 820–832.

Bendat, J. S. & Piersol, A. G. 1980 *Engineering Applications of Correlation and Spectral Analysis.* John Wiley & Sons.

Blackaby, N. D., Cowley, S. J. & Hall, P. 1993 On the instability of hypersonic flow past a flat plate. *J. Fluid Mech.* **247**, 369–416.

Boiko, A. V., Grek, G. R., Dovgal, A. V. & Kozlov, V. V. 1999 *The Generation of Turbulence in Boundary Layer Flows.* Novosibirsk, Nauka-Press (in Russian).

Boiko, A. V., Kozlov, V. V., Syzrantsev, V. V. & Shcherbakov, V. A. 1995*a* Experimental investigation of high-frequency secondary disturbances in a swept-wing boundary layer. *J. Appl. Mech. Tech. Phys.* **36**, 385–393.

Boiko, A. V., Kozlov, V. V., Syzrantsev, V. V. & Shcherbakov, V. A. 1995*b* Experimental study of the transition to turbulence at a single stationary disturbance in the boundary layer of an oblique airfoil. *J. Appl. Mech. Tech. Phys.* **36**, 67–77.

Boiko, A. V., Kozlov, V. V., Syzrantsev, V. V. & Shcherbakov, V. A. 1997 A study of the influence of internal structure of a streamwise vortex on the development of travelling disturbances inside it. *Thermophys. Aeromech.* **4**, 343–354.

Craik, A. D. D. 1971 Nonlinear resonant instability in boundary layers. *J. Fluid Mech.* **50**, 393–413.

Fu, Y. & Hall, P. 1992 Nonlinear development and secondary instability of large amplitude Görtler vortices in hypersonic boundary layers. *Eur. J. Mech.* B **11**, 465–510.

Fu, Y. & Hall, P. 1993 Effects of Görtler vortices, wall cooling and gas dissociation on the Rayleigh instability in a hypersonic boundary layer. *J. Fluid Mech.* **247**, 503–525.

Kachanov, Yu. S. 1987 On the resonant nature of the breakdown of a laminar boundary layer. *J. Fluid Mech.* **184**, 43–74.

Kachanov, Yu. S. 1994 Physical mechanisms of laminar-boundary-layer transition. *Ann. Rev. Fluid Mech.* **26**, 411–482.

Kimmel, R. L. & Kendall, J. M. 1991 Nonlinear disturbances in a hypersonic laminar boundary layer. *AIAA Paper* 91-0320.

Levchenko, V. Ya. & Shcherbakov, V. A. 1997 Instability of three-dimensional boundary layer on a swept wing. *J. Appl. Mech. Tech. Phys.* **38**, 357–363.

Mack, L. M. 1969 Boundary layer stability theory. Document 900-277, Rev. A. JPL, Pasadena, California.

Maslov, A. A. & Mironov, S. G. 1996 Experimental investigation of the hypersonic low-density flow past a half-closed cilindrical cavity. *Fluid Dyn.* **31**, 928–932.

Maslov, A. A. & Mironov, S. G. 1998 Electron-beam diagnostics of hypersonic flows. *Exp. Meas. Fluid Mech.* **12**, 4, 42–52.

Maslov, A. A., Mironov, S. G., Poplavskaya, T. V., Shiplyuk, A. N. & Vetlutsky, V. N. 1999 Viscous shock layer on a plate in hypersonic flow. *Eur. J. Mech.* B/*Fluids* **18**, 213–226.

Maslov, A. A., Mironov, S. G. & Shiplyuk, A. N. 1996*a* Experimental study of the density fluctuations in the hypersonic boundary layer on a flat plate. *J. Appl. Mech. Tech. Phys.* **37**, 816–824.

Maslov, A. A., Mironov, S. G. & Shiplyuk, A. N. 1996*b* An experimental electron-beam study of perturbations in a hypersonic shock layer on a plate. In *Proc. 8th Intl Conf. on Methods of Aerophysical Research, Novosibirsk*, part **3**, pp. 212–215. Novosibirsk.

Maslov, A. A., Mironov, S. G. & Shiplyuk, A. N. 1998 Wave processes in the hypersonic shock-layer on a flat plate. *Fluid Dyn.* **33**, 772–777.

Nayfeh, A. H. & Bozatli, A. N. 1979 Nonlinear wave interactions in boundary layers. *AIAA Paper* 79-1993.

Saric, W. S. 1994 Görtler vortices. *Ann. Rev. Fluid Mech.* **26**, 379–409.

Vetlutsky, V. N., Maslov, A. A., Mironov, S. G., Poplavskaya, T. V. & Shiplyuk, A. N. 1995 Hypersonic flow on a flat plate: Experimental results and numerical simulation. *J. Appl. Mech. Tech. Phys.* **37**, 935–943.

Vetlutsky, V. N., Mironov, S. G. & Poplavskaya, T. V. 1996 Hypersonic flow around a plate at incidence within the frames of the viscous shock layer model. In *Proc. 8th Intl Conf. on Methods of Aerophysical Research, Novosibirsk*, part **2**, pp. 221–226. Novosibirsk.